Proceedings of the 2nd Winter Workshop S&SRES'96, Polanica Zdrój 1996

GROWTH BY LHPG, STRUCTURE AND SPECTROSCOPY OF Nd^{3+}-DOPED $Ba_2NaNb_5O_{15}$NONLINEAR SINGLE-CRYSTAL FIBRES

G. Foulon, M. Ferriol, A. Brenier, M.T. Cohen-Adad and G. Boulon

Laboratoire de Physico-Chimie des Matériaux Luminescents
Unité Mixte de Recherche C.N.R.S. n° 5620
Université Claude Bernard Lyon I, Bât. 205, 43, bd. du 11 Novembre 1918
69622-Villeurbanne, Cédex, France

The renewal of the second order nonlinear crystals is very strong in laser materials optics. We are involved in the search for new systems based upon highly nonlinear niobate crystal family. Among these crystals, $Ba_2NaNb_5O_{15}$ is characterized by the highest nonlinear parameters but, unfortunately, it is difficult to grow crackless samples. The obtention of good quality and crackless $Ba_2NaNb_5O_{15}$ single crystals doped with different concentrations of Nd_2O_3 is reported. The crystals were grown as monocrystalline fibres by the laser heated pedestal growth technique. A new determination of the crystallographic structure of $Ba_2NaNb_5O_{15}$ has been performed. The structure of fibres doped with 1 at.% Nd^{3+} was found orthorhombic with the new space group $Pba2$ instead of $Cmm2$. The well-known twinning of $Ba_2NaNb_5O_{15}$ due to the exchange of the a and b axes of the unit cell, which disturbs the optical properties, decreases as the Nd^{3+} content of the fibre increases. Above 3% Nd^{3+} ions, such monocrystalline fibres were found to be of tetragonal structure. Low temperature spectroscopy reveals that Nd^{3+} ions substitute probably both Ba^{2+} and Na^{+} ions. The stimulated emission cross-section near 1060 nm of the ${}^4F_{3/2} \rightarrow {}^4I_{11/2}$ channel and its branching ratios are determined with the help of Judd–Ofelt analysis. This work shows that b-axis grown monocrystalline fibres are potentially self-doubling laser materials.

PACS numbers: 61.66.Fn, 78.20.–e

1. Introduction

Since nearly 30 years and due to its high nonlinear susceptibilities and resistance to photorefractive damage [1,2], $Ba_2NaNb_5O_{15}$ (BNN) presents interesting potential applications for optical parametric oscillation [3–7], second harmonic generation [2,8,9] or stimulated emission near 1060 nm by doping with Nd^{3+} ions [10].

However, industrial applications have not been made because high quality single crystals were difficult to obtain essentially by the Czochralski technique (CZ).

The greatest difficulty in producing good quality BNN crystals by CZ is due to the large thermal expansion of the *c* axis between 590°C and 520°C during cooling of the grown crystal leading to cracks [11]. Moreover, for undoped BNN crystals, microtwins occur on the paraelastic (tetragonal) to ferroelastic (orthorhombic) phase transition below 300°C [12] by exchange between *a* and *b* axes of the orthorhombic phase. This disturbs the crystal homogeneity and so the optical properties. The microtwinning can be avoided by cooling the crystals under an applied stress (pressure and dc voltage) from 300°C to room temperature [2, 12].

However, the cracking seems to be the most serious problem and it has been shown earlier [13] that the substitution of gadolinium for the barium and sodium in BNN reduces the thermal expansion. This suggests that doping with any trivalent rare earth ion could help to obtain good quality single crystals above all if small crystals are grown by a convenient method such as the laser heated pedestal growth (LHPG). More particularly, doping with Nd^{3+} ions would also be interesting in the aim to make a self-doubling laser material.

This article is concerned with the growth, structural characterization and spectroscopic measurements of single-crystal fibres of BNN doped with different amounts of Nd_2O_3 by the LHPG technique recently installed in our laboratory.

2. Experimental

2.1. Growth and characterization

Single-crystal fibres were grown by the LHPG technique using the furnace described elsewhere [14] from mixtures of BNN and Nd_2O_3 containing 0, 1, 2, 3, 4 and 5 at.% Nd^{3+}. A synthesis of congruently melting $Ba_2NaNb_5O_{15}$ [15] used to prepare the rods feeding the molten zone was performed as follows. Stoichiometric amounts of Nb_2O_5 (99.95%, optical grade), $Ba(NO_3)_2$ (99.99%) and Na_2CO_3 (99.95%) from Cerac were thoroughly mixed in a ball mill. The resulting powder was then cold pressed under 3000 kg cm^{-2} into disks which were annealed at 1250°C during 15 hours in an oxygen flow under 1 bar pressure. Completion of reaction was checked by X-ray powder diffractometry. The feeding rods were then obtained by grinding and mixing the BNN powder with Nd_2O_3 (99.999% from Cerac) and 0.5% of a briquetting agent (Chemplex Spectroblend powder). After cold pressing into disks 25 mm in diameter and 3–5 mm in thickness, the pellets were sintered at 650°C during 2 hours and at 1250°C for 8 hours. After cooling, they were cut into square rods about 2 × 2 mm.

The growth of fibres was performed in air atmosphere. From two ceramic rods as a feed and seed the pulling led to randomly oriented crystals. After orientation by X-ray Laue diffractometry, a *b*-axis oriented crystal was pulled by mounting the as-grown crystal used as a seed at an appropriate angle to the growth direction. The laser power was in the 16 to 30 W range without attenuation. The pulling rates ranged between 30 and 40 mm h^{-1}. The ratio of pulling and feeding rates was chosen to obtain fibres with a diameter between 400 and 800 μm. The length of

the fibres was between 20 and 70 mm. Finally, the fibres were annealed at 1200°C during 10 hours under an oxygen flow.

External and internal morphology of the as-grown fibres was performed by optical microscopy (LEICA DMR–RXE) after mechanical polishing and etching with a HF/HNO_3 mixture (1:2 by volume) at 80°C during 10 min. Under optical microscopic examination all fibres exhibited no cracks with a cross-section practically circular with two opposite growth ridges.

Twinning was characterized by Raman polarized microspectroscopy (DILOR XY) at room temperature.

Quantitative analyses for Nd, Na, Ba and Nb along the pulled fibres were made after embedding in epoxy resin and mechanical polishing, by energy dispersion of X-ray (JEOL 840 ALGS microscope, EDX TRACOR microprobe) taking the intensities of K lines for Na and of L lines for Nd, Ba and Nb with an accelerating tension of 15 kV and a take-off angle of 40°C. Measurements were made using precalibrated internal standards and corrected by the ZAF method. Despite an accuracy of measurements within 3%, the strong overlapping of Nd and Ba L-lines combined with a small ratio Nd/Ba allowed us to determine only relative variations and not absolute values of the Nd content.

Excitation of the Nd^{3+} luminescence was performed with a laser analytical systems dye laser pumped by a frequency-doubled Nd:YAG laser from BM INDUSTRIES. The detection of the luminescence was carried out through a JOBIN–YVON JYHRS2 monochromator fitted with a 1 μm blazed grating (2.4 nm resolution/mm slits) and a R1767 HAMAMATSU photomultiplier. The signal was sent in a Stanford boxcar averager SRS 250. The decay kinetics was recorded with a digital LECROY 9410 oscilloscope.

3. Results and discussion

3.1. Raman microspectrometry

Twinning of undoped BNN monocrystalline fibres was evidenced by Raman microspectrometry. The notation used to classify the recorded spectra was the following: *excitation direction (excitation polarization, emission polarization) emission direction.* Figure 1 shows the evolution of $Z(YY)Z$ and $Z(XX)Z$ spectra along a fibre. An inversion of the shape of the spectra can be clearly seen corresponding to an inversion of the polarization related to the exchange between a and b axes. It must be noticed that this is a macroscopic study with no relation with the real periodicity of the phenomenon.

3.2. EDX analysis

Fibres with 4 at.% Nd^{3+} in the feed rod were analyzed by energy dispersion of X-ray (EDX) microanalysis. No significant variations of Na, Ba, Nb and Nd contents were obtained on the whole length of the analyzed fibres. This indicates that our growth conditions ensure the chemical homogeneity of the crystal and that the effective distribution coefficient of each species is therefore close to one.

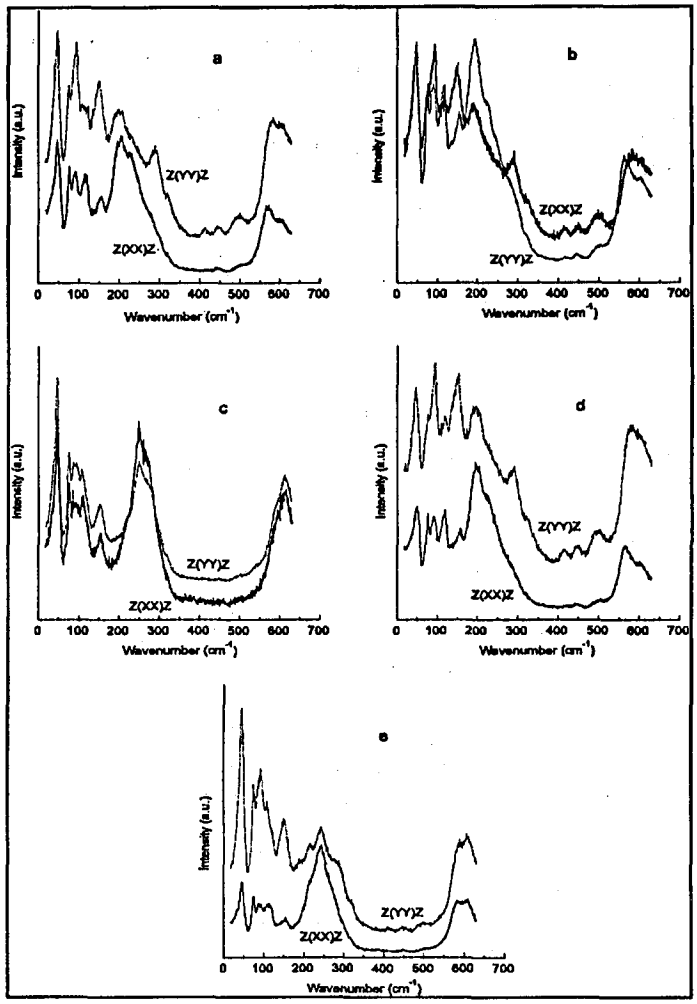

Fig. 1. Raman microspectroscopy of an undoped BNN single-crystal fibre; (a) — beginning of the fibre, (b) — first quarter of the fibre, (c) — half of the fibre, (d) — third quarter of the fibre, (e) — end of the fibre.

3.3. Crystallographic structure

In order to perform an accurate structural determination in the orthorhombic system, a data collection on a 1 at.% Nd^{3+} doped BNN fibre was done (ENRAF NONIUS CAD 4 Diffractometer). The quality of such a fibre was much better than the quality of the pure BNN fibres which were twinned.

Contrary to the space group mentioned in the literature, i.e. *Cmm*2 [16], the data collection analysis gave *Pba*2 as a space group for 1 at.% Nd^{3+} doped $Ba_2NaNb_5O_{15}$. This hypothesis was confirmed by a subsequent development of the structure and a rather low reliability factor. We also assume *Pba*2 as a space group for undoped BNN.

$Ba_2NaNb_5O_{15}$ crystallizes with the tungsten bronze structure which contains five kinds of cations sites. The first, classically denoted A1 is of square section, 12-fold coordinated and filled by Na^+ ions with a mean degree occupancy of 0.5. The second A2 is of pentagonal section, 15-fold coordinated and filled by Ba^{2+} ions (mean occupancy factor: 1). The third, C, has a small triangular section and is empty. These sites are linked with two kinds of NbO_6 octahedra denoted B1 and B2. Considering its rather large ionic radius, we expect that the Nd^{3+} ion could be located at least in A1 and A2 sites and, in any case, we expect different Nd^{3+} environments which can be revealed by low temperature spectroscopy.

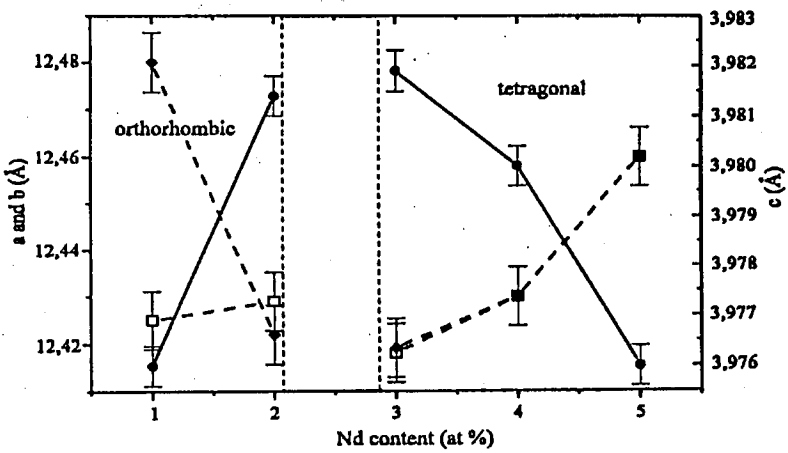

Fig. 2. Evolution of cell parameters of BNN single-crystal fibres as a function of neodymium content (□: *a* axis, ◇: *b* axis, •: *c* axis).

The lattice parameters have been measured as a function of the neodymium content of the fibres at room temperature (Fig. 2). It can be seen that a change between orthorhombic (space group: *Pba*2) and tetragonal (space group: *P*4*bm*) symmetry occurs at a doping level between 2 and 3 at.% Nd^{3+}. In terms of symmetry [17], this result reinforces the hypothesis of *Pba*2 as the right space group for undoped BNN crystals. Possibly, the temperature of the paraelastic (tetragonal) to ferroelastic (orthorhombic) transition occurring below 300°C in undoped BNN [12] is Nd^{3+} concentration dependent and takes place below room temperature above 2 at.% Nd^{3+}. Investigations are in progress to validate this hypothesis.

The value of 3 at.% Nd^{3+} corresponds also to a maximum crystal quality due to the progressive disappearance of microtwins and to the fact that above 3%, X-ray measurements showed that the crystal quality tended to a slight decrease. Therefore, the best Nd^{3+} content for optical applications (self-doubling laser material) appears to lie in this range.

3.4. Laser spectroscopy of Nd^{3+}-doped $Ba_2NaNb_5O_{15}$

3.4.1 Neodymium sites

In order to excite all the Nd^{3+} sites, we have obtained under broad band excitation in the 860-880 nm range corresponding to the $^4I_{9/2} \rightarrow {}^4F_{3/2}$ transition, the spectrum at low temperature (6 K) corresponding to the $^4F_{3/2} \rightarrow {}^4I_{11/2}$ transition represented in Fig. 3. We can see a peak at 1054.5 nm and a group of peaks near 1060 nm. The fluorescence in the peak at 1054.5 nm has a decay time of 290 μs and the peaks near 1060 nm have a decay time of 180 μs, each decay being measured under laser excitation at an appropriate wavelength given by the laser excitation spectrum of the considered peak of fluorescence. It means that at least two individual Nd^{3+} sites have been excited. In addition, the broadening of the emission spectrum at 6 K reveals large inhomogeneous broad lines associated with multicentre distributions.

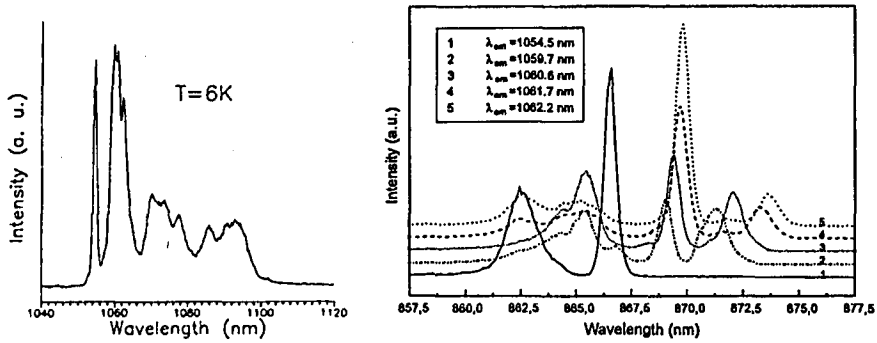

Fig. 3. Nd^{3+} low temperature emission spectrum corresponding to the $^4F_{3/2} \rightarrow {}^4I_{11/2}$ transition obtained under broad band excitation in the $^4F_{3/2}$ level.

Fig. 4 Low temperature (6 K) laser excitation spectra of different Nd^{3+} emission wavelengths corresponding to the $^4F_{3/2} \rightarrow {}^4I_{11/2}$ transition.

The excitation spectra represented in Fig. 4 are recorded under monitoring of different parts of the $^4F_{3/2} \rightarrow {}^4I_{11/2}$ emission spectrum. Moreover, the decays are exponential giving no evidence of energy transfer between Nd^{3+} sites. The range of the excitation spectra is 860–880 nm corresponding to the $^4I_{9/2} \rightarrow {}^4F_{3/2}$ transition so that at low temperature we expect two lines R_1 and R_2 from the lowest level of the $^4I_{9/2}$ ground state for each individual Nd^{3+} site as shown in the scheme of levels in Fig. 5. It should be mentioned that such monitoring should reveal the doublet structure of the $^4F_{3/2}$ level belonging to one individual site. The excitation spectra of Fig. 4 contain sometimes up to four main peaks more or less broad traducing that different Nd^{3+} sites exist and can emit at the same wavelength. A more understandable picture of the different peaks present in the excitation spectra of Fig. 4 is given in Fig. 5. These two figures show that peaks in the excitation spectra move continuously when the monitored emission wavelength is moved continuously, giving rise to families of peaks. In order to assign each peak

to an R_1 or R_2 transition with the R_2 energy higher than the R_1 one, we have excited the sample at liquid helium temperature with laser wavelengths in the range 862–874 nm and for each laser wavelength we have monitored the emission ($^4F_{3/2} \rightarrow {}^4I_{9/2}$ transition) which wavelength was in coincidence with the one of the excitation laser. Let us recall that, at low temperature, only the lowest sublevel of $^4F_{3/2}$ can emit so that an R_2 excitation can be distinguished from an R_1 one because it leads to no emission at the same wavelength.

For wavelengths shorter than 866 nm the fluorescence in coincidence with the laser line is hardly seen indicating that peaks located below 866 nm in Fig. 5 can hardly be assigned to R_1 lines. For wavelengths higher than 866 nm the fluorescence in coincidence with the laser line is clearly seen (indicating that peaks in Fig. 5 above 866 nm can be assigned to R_1 lines) and its laser excitation spectrum contains peaks at short wavelengths, below 866 nm, confirming the R_2 assignment to peaks below 866 nm in Fig. 5. The assignments of the peaks are represented by squares and triangles in Fig. 5 and our conclusion based upon the presence of many R_1 excitations is the existence of many Nd^{3+} environments in our BNN crystal fibres which we shall now try to relate to the crystallographic cation sites of the tungsten bronze structure.

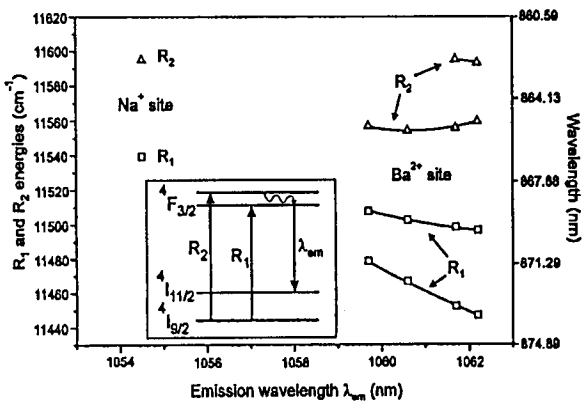

Fig. 5. Main peaks in the laser excitation spectra (6 K) of the Nd^{3+} emission peaks corresponding to the $^4F_{3/2} \rightarrow {}^4I_{11/2}$ transition and their interpretation.

Because the sodium A1 site has a centre of inversion if we consider the 12 oxygen first neighbors suppressing electric-dipole transitions and that the barium A2 site has no centre of inversion allowing electric-dipole transitions and so, shortening the fluorescence decay time, we formulate the hypothesis that the Nd^{3+} ions emitting at 1054.5 nm with the longer decay time are located in sodium A1 sites whereas Nd^{3+} ions emitting near 1060 nm are located in barium A2 sites. In this case, the different R_1 lines observed in Figs. 4 and 5 could be due to the fact that the Nd^{3+}[A2] can have an A1 neighbor site which can be empty or Na^+ occupied. Possibly, these two situations are related to the two families of R_1 lines exhibited in Fig. 5 and corresponding to the emissions near 1060 nm, the Nd^{3+} distribu-

tion being random. Moreover, large vibrations of the Nd^{3+} ions inside the barium A2 sites could contribute to the broadening of the emission peaks observed near 1060 nm.

On the other hand, the emission near 1060–1062 nm and originating from the 862.5–866 nm excitation could be partly due to Nd^{3+} ions in A1 sites because the Nd^{3+} emission spectrum extends up to 1100 nm and is not located in only one peak at 1054.5 nm. Nevertheless, we have obtained no evidence of Nd[A1]→Nd[A2] energy transfers because the observed Nd[A1] decays were exponential and no initial rise-time was observed in the Nd[A2] fluorescence.

3.4.2 Branching ratios and emission cross-sections

We have calculated the branching ratios of the $^4F_{3/2}$ fluorescences of Nd^{3+} in BNN fibres with the procedure developed in Ref. [18] and based upon Judd–Ofelt theory [19,20]. In Ref. [18], it is shown that knowledge of the ratio $X \cong \Omega_4/\Omega_6$ of the two intensity parameters is sufficient for calculating the four branching ratios $\beta_{0.9}$, $\beta_{1.06}$, $\beta_{1.35}$ and $\beta_{1.9}$ corresponding to the transitions from $^4F_{3/2}$ to respectively $^4I_{9/2}$, $^4I_{11/2}$, $^4I_{13/2}$ and $^4I_{15/2}$. Preliminarily, we have obtained the ratio X using the following formula [18]:

$$X = (0.2874S - 0.07671)/(0.3194 - 0.1053S), \tag{1}$$

where S is the ratio of the measured intensities (photons/s) of the fluorescences corresponding to the $^4F_{3/2} \rightarrow {}^4I_{9/2}$ transition (near 900 mn) and $^4F_{3/2} \rightarrow {}^4I_{11/2}$ transition (near 1060 nm). We have measured $S = 0.8767$ and this value, inserted in (1), produces $X = 0.7717$. Then using expressions given in Ref. [18], we have obtained $\beta_{0.9} = 0.412$, $\beta_{1.06} = 0.47$, $\beta_{1.35} = 0.115$ and $\beta_{1.9} = 0.00294$.

The Nd^{3+} stimulated emission cross-section $\sigma_e^{\pi/\sigma}(\omega)$ at frequency ω and in polarization π or σ corresponding to the $^4F_{3/2} \rightarrow {}^4I_{11/2}$ transition was obtained through the McCumber relation [21]

$$\sigma_e^{\pi/\sigma}(\omega) = f^{\pi/\sigma}(\omega)(2\pi c/\omega n^{\pi/\sigma})^2, \tag{2}$$

where $n^{\pi/\sigma}$ are respectively the extraordinary and ordinary refractive indexes and where the experimental emission spectra $f^{\pi/\sigma}(\omega)$ are normalized such that

$$\beta_{1.06}/\tau = (8\pi/3)\int (2f^{\sigma} + f^{\pi})\mathrm{d}\omega/2\pi, \tag{3}$$

where τ is the radiative lifetime of the $^4F_{3/2}$ level at room temperature. Because the measured lifetime, at room temperature, of the $^4F_{3/2}$ level (180 μs) at 1060 nm associated only with Nd[A2] sites is the same as the one measured at liquid helium temperature, no quenching occurs at least up to room temperature. The situation is very similar to the one in $LiNbO_3$:MgO:Nd^{3+} [22] and we have used 180 μs in (3) as the radiative lifetime of $^4F_{3/2}$ level at room temperature. The result of (2) is the stimulated emission cross-section for the $^4F_{3/2} \rightarrow {}^4I_{11/2}$ transition given in Fig. 6. The σ polarization of the ordinary wave only needs to be considered for self-doubling laser operation with birefringent phase matching. However, we can see in Fig. 6 that its intensity is weaker than for π polarization but still stays high enough to be applied.

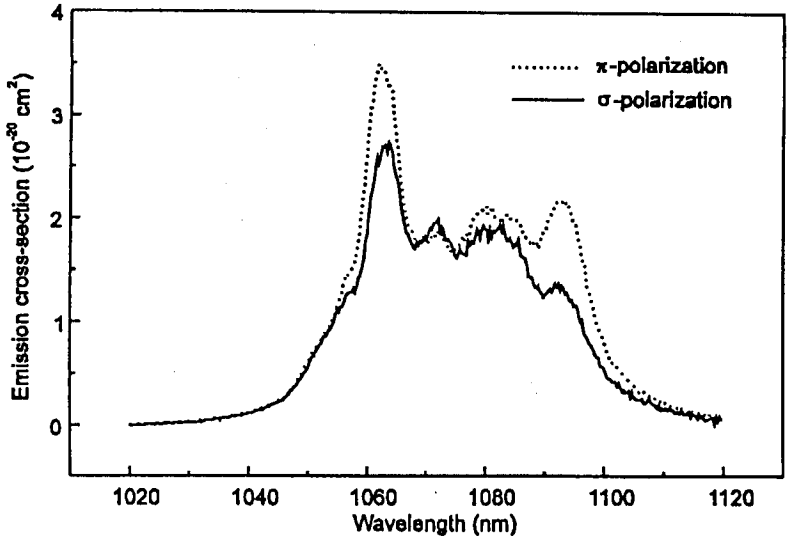

Fig. 6. Stimulated emission cross-section corresponding to the ${}^4F_{3/2} \rightarrow {}^4I_{11/2}$ transition of the Nd^{3+} ion in a $Ba_2NaNb_5O_{15}$ single-crystal fibre.

4. Conclusion

The LIIPG technique is a useful tool as a material supplier in the field of laser crystals especially when the research of optical properties needs different compositions of the host and several concentrations of dopants. With this technique we have obtained crackless Nd^{3+}-doped $Ba_2NaNb_5O_{15}$ fibres of good crystalline quality.

Their space group has been found *Pba*2 different of the one published in the literature (*Cmm*2) concerning crystals grown by the Czochralski method. As this space group corresponds to a slight distortion of the tetragonal structure (space group *P*4*bm*) we have shown that it is possible to return to the stable tetragonal configuration of the tungsten-bronze-type structure by introducing a sufficient amount of Nd^{3+} ions (3 at.%). A consequence of this phenomenon is to avoid the formation of microtwins which have been prejudicial in the past to the good optical quality of crystals grown by the Czochralski technique.

Low temperature spectroscopic measurements have shown that Nd^{3+} ion are mainly located in two different non-equivalent positions in relation to the existence of Ba^{2+} and Na^+ sites in the tungsten-bronze structure. The Nd^{3+} stimulated emission cross-section at 1060 nm, corresponding to the [A2] sites at room temperature, has been found to be reasonably high so that Nd^{3+}-doped $Ba_2NaNb_5O_{15}$ crystal fibres are an attractive self-doubling laser material.

References

[1] J.E. Geusic, H.J. Levinstein, J.J. Rubin, S. Singh, L.G. Van Uitert, *Appl. Phys. Lett.* 11, 269 (1967).

[2] S. Singh, D.A. Draegert, J.E. Geusic, *Phys. Rev. B* 2, 2709 (1970).

[3] R.G. Smith, J.E. Geusic, H.J. Levinstein, J.J. Rubin, S. Singh, L.G. Van Uitert, *Appl. Phys. Lett.* **12**, 308 (1968).

[4] S.A. Baryshev, V.I. Pryalkin, A.I. Kholodnykh, *Sov. Phys. Lett.* **6**, 415 (1980).

[5] G.I. Onischukov, A.A. Formichev, A.I. Kholodnykh, *Sov. J. Quant. Electr.* **13**, 1001 (1983).

[6] G. Ionushauskas, A. Piskarskas, V. Sirutkaitis, A. Yuozapavichyus, *Sov. J. Quant. Electr.* **17**, 1303 (1987).

[7] A. Piskarskas, V. Smilgevicius, A. Umbrasas, *Opt. Commun.* **73**, 322 (1989).

[8] W. Culshaw, J. Kannelaud, J.E. Peterson, *I.E.E.E. J. Quant. Electr.* **QE10**, 263 (1974).

[9] S.R. Chinn, *Appl. Phys. Lett.* **29**, 176 (1976).

[10] A.A. Kaminskii, V.A. Koptsik, Y.A. Maskaev, I.I. Naumova, L.N. Rashkovich, S.E. Sarkisov, *Phys. Status Solidi A* **28**, K5 (1975).

[11] A.A. Ballman, J.R. Carruthers, B. O'Bryan, *J. Cryst. Growth* **6**, 184 (1970).

[12] L.G. Van Uitert, J.J. Rubin, W.A. Bonner, *I.E.E.E. J. Quant. Electr.* **QE4**, 622 (1968).

[13] W. Shimazu, M. Tsukioka, N. Mitobe, S. Kuroiwa, S. Tsutsumi, *J. Mater. Sci.* **25**, 4525 (1990).

[14] G. Foulon, M. Ferriol, A. Brenier, M.T. Cohen-Adad, G. Boulon, *Chem. Phys. Lett.* **245**, 555 (1995).

[15] B.A. Scott, E.A. Giess, D.F. O'Kane, *Matter. Res. Bull.* **4**, 107 (1969).

[16] J.J. Rubin, L.G. Van Uitert, J.H. Levinstein, *J. Cryst. Growth* **1**, 315 (1967).

[17] *International Tables for Crystallography*, Ed. T. Hahn, 2nd ed. Vol. A, International Union of Cristallography, Kluwer Academic Publishers, Dordrecht 1987.

[18] T.S. Lomheim, L.G. Deshaser, *Opt. Commun.* **24**, 89 (1978).

[19] B.R. Judd, *Phys. Rev.* **127**, 750 (1962).

[20] G.S. Ofelt, *J. Chem. Phys.* **37**, 37 (1962).

[21] D.E. Mccumber, *Phys. Rev.* **136**, 954 (1964).

[22] T.Y. Fan, A. Cordova-Plaza, M.J.F. Digonnet, R.L. Byer, H.J. Shaw, *J. Opt. Soc. Am. B* **3**, 140 (1986).